Electron-Rich Diplatinum(0) Metallocryptate Promoting Novel Successive Encapsulation of Acidic Hydrides

Eri Goto,[†] Miho Usuki,[†] Hiroe Takenaka,[†] Ken Sakai,[‡] and Tomoaki Tanase*,[†]

Department of Chemistry, Faculty of Science, Nara Women's University, Kitauoya-higashi-machi, Nara 630-8285, Japan, and Department of Applied Chemistry, Faculty of Science, Tokyo University of Science, Shinjuku-ku, Tokyo 162-8601, Japan

Received June 21, 2004

Reaction of $[Pt(XylNC)_4](PF_6)_2$ with $NaBH_4$ in the presence of 2,7-bis(diphenylphosphino)-1,8-naphthyridine (dpnapy) afforded a diplatinum(0) metallocryptate with a tightly encapsulated sodium ion in a pseudo-D_3 helical cage, $[Pt_2Na(\mu\text{-dpnapy})_3(XylNC)_2](PF_6)$ (**4a**; XylNC = 2,6-xylyl isocyanide). The three linear dpnapy ligands in complex **4a** are bundled by a sodium ion through six Na−N bonds, and two $Pt^0(XylNC)$ fragments cap each end of the double-tripodal $\{(dpnapy)_3Na\}^+$ unit through three Pt−P bonds. Each electron-rich platinum(0) center adopts a tetrahedral geometry with 18 valence electrons. An analogous dipalladium(0) complex, $[Pd_2Na(\mu\text{-dpnapy})_3(XylNC)_2](PF_6)$ (**4b**), was prepared by reaction of $[Pd_3(XylNC)_6]$ with dpnapy and $NaPF_6$. The terminal isocyanide ligands of complexes **4a**,**b** were readily replaced by CO (1 atm) to give $[M_2Na(\mu\text{-dpnapy})_3(CO)_2](PF_6)$ (M = Pt (**4c**), Pd (**4d**)). In the presence of H^+ ions, the electron-rich diplatinum metallocryptate **4a** interestingly demonstrated successive encapsulation of protons as platinum-bound hydrides, resulting in the formation of $[Pt_2Na(H)(\mu\text{-dpnapy})_3(XylNC)_2](PF_6)_2$ (**5**) and $[Pt_2Na(H)_2(\mu\text{-dpnapy})_3(XylNC)_2](PF_6)_3$ (**6**). Complexes **5** and **6** were isolated from alternative reactions of $[Pt_3(XylNC)_6]$ with dpnapy and $NaPF_6$ in the presence of regulated amounts of HPF_6. Whereas the structures of **5** and **6** are closely similar to that of **4a**, one and two hydrides are trapped into the small room comprised of the $\{Pt(PCN)_3Na\}$ framework in complexes **5** and **6**, respectively. The hydride attached to the Pt center at the opposite site of isocyanide with the Pt atom deformed slightly toward trigonal-bipyramidal geometry. The structure of **5** is asymmetric with the hydride fixed onto a platinum center, and any site-exchange behavior of the hydride was not observed even in solution. The hydride encapsulation in **5** drags the encountered platinum atom inside by ca. 0.17 Å and causes slight but appreciable distortion around the central Na ion with an average Na−N distance of 2.42 Å for the Pt^0 side and 2.54 Å for the PtH side. The structural distortion caused by the hydride encapsulation might have influenced the other Pt center to be less reactive and stabilize the asymmetric structure of **5**. Electrochemical measurements for **4a**, **5**, and **6** were performed to reveal that complex **4a** underwent two irreversible one-electron oxidation processes at $E_{pa}{}^1 = -0.14$ V (vs Ag/Ag^+) and 0.15 V, corresponding to $Pt^0{}_2 \rightarrow Pt^0Pt^I \rightarrow Pt^I{}_2$ with some concomitant structural changes, and the hydride encapsulation made the Pt center redox inactive in **5** and **6**, as $Pt^0(PtH) \rightarrow Pt^I(PtH)$ (**5**) and $(PtH)_2$ were redox silent (**6**).

Introduction

Multinuclear heterometallic complexes have been regarded as one of the valuable motifs in developing multifunctional catalytic systems and electro- and photochemical devices.[1] Utilization of appropriately designed supporting ligands with heterodonor atoms is of synthetic importance to assemble the heterometal atoms in desired arrangements. In this context, easily available PNNP ligands, such as 2,9-bis(diphenylphosphino)-1,10-phenanthroline (P_2phen), 6,6′-bis(diphenylphosphino)-2,2′-bipyridine (P_2bpy), 3,6-bis(diphenylphosphino)-pyridazine (P_2pz), and 2,7-bis(diphenylphosphino)-1,8-naphthyridine (dpnapy), have been used to construct $\{M(\mu\text{-PNNP})_3M\}$ metallocryptands which encapsulate a heterometal atom in the cage.[2−9] Catalano et al. have

* To whom correspondence should be addressed. E-mail: tanase@cc.nara-wu.ac.jp.
[†] Nara Women's University.
[‡] Tokyo University of Science.

(1) (a) *Catalysis by Di- and Polynuclear Metal Cluster Complexes*; Adams, D. A., Cotton, F. A., Eds.; Wiley-VCH: New York, 1998. (b) Balch, A. L. In *Homogeneous Catalysis with Metal Phosphine Complexes*; Pignolet, L. H., Ed.; Plenum Press: New York, 1983; p 167. (c) Sinfelt, J. H. *Bimetallic Catalysis: Discoveries, Concepts and Applications*; Wiley: New York, 1983. (d) Guczi, L. In *Metal Clusters in Catalysis*; Gates, B. C., Guczi, L., Knozinger, H., Eds.; Elsevier: New York, 1986. (e) Farrygia, L. J. *Adv. Organomet. Chem.* **1990**, *31*, 301. (f) Braunstein, P.; Rose, J. In *Comprehensive Organometallic Chemistry II*; Adams, R. D., Ed.; Elsevier: New York, 1995; Vol. 10, p 351.

(2) Catalano, V. J.; Bennett, B. L.; Malwitz, M. A.; Yson, R. L.; Kar, H. M.; Muratidis, S.; Horner, S. J. *Comments Inorg. Chem.* **2003**, *24*, 39.

(3) (a) Catalano, V. J.; Bennett, B. L.; Kar, H. M. *J. Am. Chem. Soc.* **1999**, *121*, 10235. (b) Catalano, V. J.; Bennett, B. L.; Noll, B. C. *Chem. Commun.* **2000**, 1413. (c) Catalano, V. J.; Bennett, B. L.; Yson, R. L.; Noll, B. C. *J. Am. Chem. Soc.* **2000**, *122*, 10056. (d) Catalano, V. J.; Malwitz, M. A.; Noll, B. C. *Chem. Commun.* **2001**, 581. (e) Catalano, V. J.; Malwitz, M. A.; Noll. B. C. *Inorg. Chem.* **2002**, *41*, 6553.

10.1021/om049548v CCC: $27.50
Publication on Web 11/03/2004

Chart 1

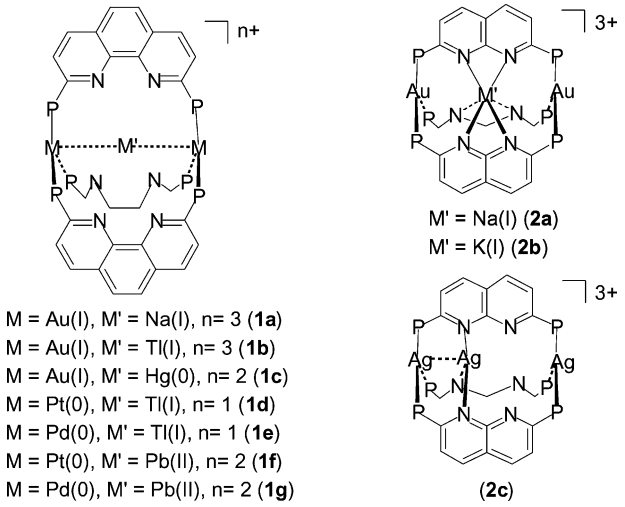

M = Au(I), M' = Na(I), n= 3 (**1a**)
M = Au(I), M' = Tl(I), n= 3 (**1b**)
M = Au(I), M' = Hg(0), n= 2 (**1c**)
M = Pt(0), M' = Tl(I), n= 1 (**1d**)
M = Pd(0), M' = Tl(I), n= 1 (**1e**)
M = Pt(0), M' = Pb(II), n= 2 (**1f**)
M = Pd(0), M' = Pb(II), n= 2 (**1g**)

Scheme 1

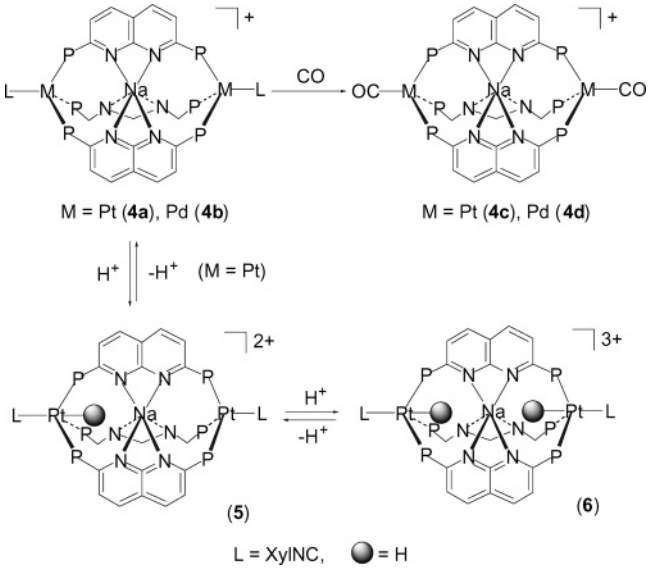

prepared a series of the metallocryptates $[M_2M'(\mu\text{-}P_2\text{phen})_3]^{n+}$, in which two d^{10} metals, Au(I), Ag(I), Pt(0), and Pd(0), capped the three P_2phen ligands with a 16-valence-electron, triangular $[MP_3]$ geometry, forming a relatively large cavity. A heterometal M′ of Na(I), Tl(I), or Pb(II) is trapped in the cage by an attractive interaction between closed-shell metal ions/atoms rather than direct interaction with the phenanthroline N donors.[2,3] Isolated and characterized examples are $[Au_2M'(\mu\text{-}P_2\text{phen})_3]^{3+}$, (M′ = Na (**1a**), Tl (**1b**)), $[Au_2Hg(\mu\text{-}P_2\text{phen})_3]^{2+}$ (**1c**), $[M_2Tl(\mu\text{-}P_2\text{phen})_3]^{+}$ (M = Pt (**1d**), Pd (**1e**)), and $[M_2Pb(\mu\text{-}P_2\text{phen})_3]^{2+}$ (M = Pt (**1f**), Pd (**1g**)) (Chart 1).[3] The large cavity comprised of the $[M_2(\mu\text{-}P_2\text{phen})_3]$ framework (M = Pt, Pd) is also able to encapsulate a spinning Hg_2^{2+} dimer.[3e] In contrast, the linearly ordered PNNP ligand, dpnapy, has the potential to construct rigid and small cages with a $\{M(\mu\text{-dpnapy})_3M\}$ framework and encapsulation of heteroatoms into the cage could afford linear multimetallic aggregations;[5−8] however, only a few examples of multinuclear complexes with dpnapy ligands have been reported with $[Au_2M'(\mu\text{-dpnapy})_3]^{3+}$ (M′ = Na (**2a**),[7] K (**2b**)[6]) (Scheme 1), $[Ag_3(\mu\text{-dpnapy})_3]^{3+}$ (**2c**),[6,7] and *trans-/cis*-$[Mo_2(\mu\text{-}CH_3COO)_2(\mu\text{-dpnapy})_2]^{2+}$ (**3**).[8] In complexes **2a**,**b**, two trigonal Au(I) ions are coordinated by three phosphine groups of the dpnapy ligands and the sodium or potassium ion is tightly held at the center of a D_3-symmetrical small cavity through six bonding interactions with the imine nitrogen atoms. Notably, all capping units of complexes **1** and **2** are trigonal-planar d^{10} metals with 16 valence electrons, which could not react with another ligand toward 18-valence-electron, tetrahedral metal centers.

We wish to report herein the synthesis and characterization of the electron-rich diplatinum(0) and dipalladium(0) metallocryptate of dpnapy with a sodium ion nesting at the center of the cage, $[M_2Na(\mu\text{-dpnapy})_3(L)_2]^{+}$ (M = Pt, Pd; L = 2,6-xylyl isocyanide (XylNC), CO), and novel successive encapsulation of acidic hydrides into the rigid cavity of $[Pt_2Na(\mu\text{-dpnapy})_3(XylNC)_2]^{+}$ (**4a**).

Results and Discussion

Syntheses of d^{10} Dinuclear Complexes with dpnapy, $[M_2Na(\mu\text{-dpnapy})_3(XylNC)_2](PF_6)$ (M = Pt (4a), Pd (4b)). When the platinum(II) complex $[Pt(XylNC)_4](PF_6)_2$ was treated with dpnapy in the presence of $NaBH_4$ in ethanol, violet microcrystals of $[Pt_2Na(\mu\text{-dpnapy})_3(XylNC)_2](PF_6)$ (**4a**) were isolated in good yields (Scheme 1). A similar reaction by using $[Pd(XylNC)_4](PF_6)_2$ failed to result in an analogous complex; however, reaction of the palladium(0) cluster $[Pd_3(XylNC)_6]$ with stoichiometric amounts of dpnapy and $NaPF_6$ afforded $[Pd_2Na(\mu\text{-dpnapy})_3(XylNC)_2](PF_6)$ (**4b**) in good yields. The IR spectra of **4a** and **4b** indicated the presence of terminal isocyanides with the N≡C stretching bands at 2048 (**4a**) and 2061 (**4b**) cm^{-1}, corresponding to isocyanide ligands bound to zerovalent Pt and Pd centers.[9] In the ^1H NMR spectra, a singlet resonance for *o*-methyl protons of XylNC was observed at δ 1.95 ppm (**4a**) and 1.94 ppm (**4b**) and the naphthyridine protons symmetrically appeared as two doublets at δ 6.43 and 7.40 ppm ($^3J_{HH}$ = 8.3 Hz) for **4a** and δ 6.54 and 7.47 ppm ($^3J_{HH}$ = 8.4 Hz) for **4b**. The peak intensities for the methyl and aromatic protons suggested that the ratio of XylNC and dpnapy is 2:3. The $^{31}P\{^1H\}$ NMR spectrum of complex **4a** exhibited a singlet peak at δ 23.3 ppm with ^{195}Pt satellite peaks of $^1J_{PtP}$ = 3850 Hz (Figure 1), and the same peak appeared as a singlet at δ 26.7 ppm for **4b**. These spectral features are suggestive of highly symmetrical environments of the metallocryptate complexes **4a**,**b**. The ESI mass spectra of **4a**,**b** measured in dichloromethane are consistent with a metallocryptate structure including sodium. The mass spectrum of **4a** showed an intense divalent peak at *m/z* 1020.19 corresponding to $\{[Pt_2Na(dpnapy)_3(XylNC)] + H\}^{2+}$, and that of **4b** showed an

(4) (a) Catalano, V. J.; Kar, H. M.; Garnas, J. *Angew. Chem., Int. Ed.* **1999**, *38*, 1979. (b) Catalano, V. J.; Malwitz, M. A.; Horner, S. J.; Vasquez, J. *Inorg. Chem.* **2003**, *42*, 2141. (c) Kuang, S.-M.; Zhang, L.-M.; Zhang, Z.-Z.; Wu, B.-M.; Mak, T. C. W. *Inorg. Chim. Acta* **1999**, *284*, 278.

(5) Ziessel, R. *Tetrahedron Lett.* **1989**, *30*, 463.

(6) Uang, R.-H.; Chan, C.-K.; Peng, S.-M.; Che, C.-M. *J. Chem. Soc., Chem. Commun.* **1994**, 2561.

(7) Catalano, V. J.; Kar, H. M.; Bennett, B. L. *Inorg. Chem.* **2000**, *39*, 121.

(8) Tanase, T.; Igoshi, T.; Kobayashi, K.; Yamamoto, Y. *J. Chem. Res., Synop.* **1998**, 538.

(9) Tanase, T.; Horiuchi, T.; Yamamoto, Y.; Kobayashi, K. *J. Organomet. Chem*. **1992**, *440*, 1.

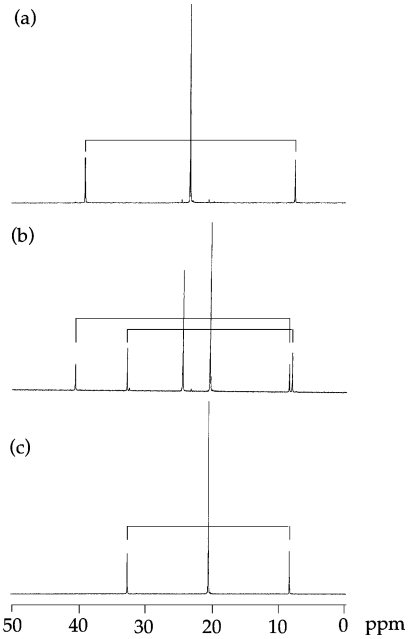

Figure 1. $^{31}P\{^{1}H\}$ NMR spectra of the dpnapy region for (a) **4a**, (b) **5**, and (c) **6** in CD_2Cl_2 at room temperature.

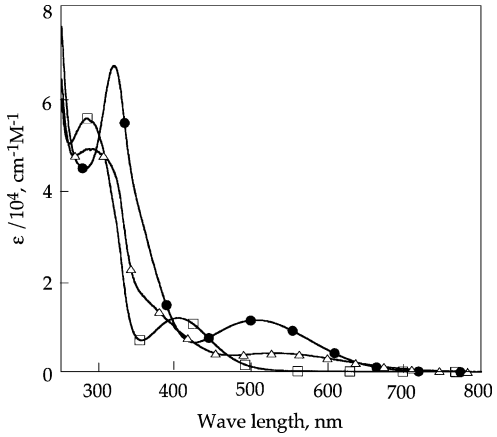

Figure 2. Electronic absorption spectra of **4a** (●), **5** (△), and **6** (□) in dichloromethane at room temperature.

intense monocation peak at *m/z* 1731.25 assignable to $[Pd_2Na(dpnapy)_3(XylNC)_2]^+$. The electronic absorption spectra of **4a**,**b** are closely similar to each other, showing a very broad band around 505 nm and an intense band at ca. 315 nm (Figure 2).

Structures of $[M_2Na(\mu\text{-dpnapy})_3(XylNC)_2](PF_6)$ (M = Pt (4a), Pd (4b)). The detailed structure of complex **4a** was determined by X-ray crystallography; an ORTEP plot for the complex cation is given in Figure 3, and selected bond distances and angles are summarized in Table 1. The complex cation of **4a** is comprised of two platinum atoms bridged by three dpnapy ligands to form a $\{Pt_2(dpnapy)_3\}$ framework, which is further coordinated by two terminal isocyanide ligands. In addition, a sodium ion is tightly encapsulated at the center of the D_3-symmetrical $\{LPt(dpnapy)_3PtL\}$ cage (L = XylNC) through six imino N atoms (average Na−N = 2.45 Å). The encapsulated structure of a sodium ion by three dpnapy ligands is closely similar to that found in the dinuclear Au(I) metallocryptate with dpnapy, $[Au_2Na(\mu\text{-dpnapy})_3](PF_6)_3$ (**2a**) (average Na−N = 2.46 Å).[7] The two platinum atoms sit in identical

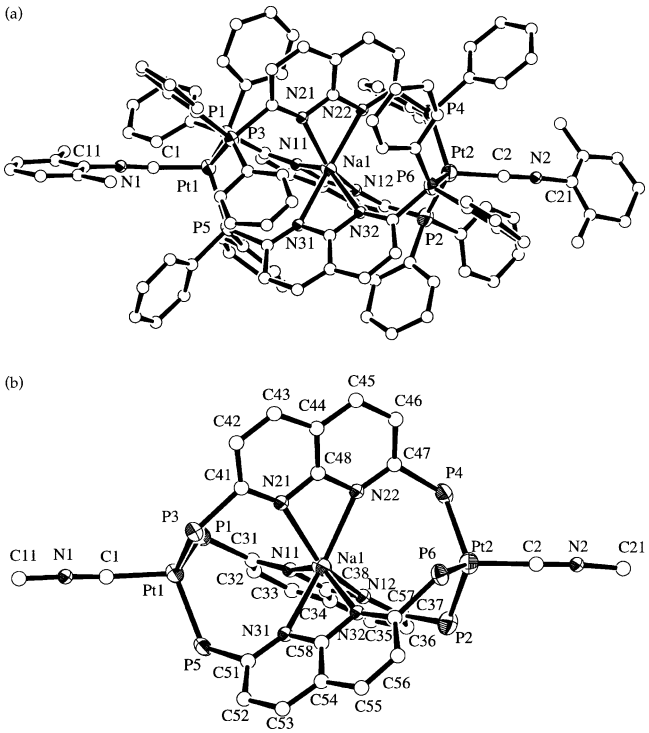

Figure 3. (a) ORTEP plot for the complex cation of **4a**·$2CH_2Cl_2$·$2H_2O$, $[Pt_2Na(\mu\text{-dpnapy})_3(XylNC)_2]^+$. The carbon and nitrogen atoms are drawn with ideal circles for clarity. (b) ORTEP view for the complex framework of **4a**, the phenyl and xylyl rings being omitted for clarity.

Table 1. Selected Bond Lengths (Å) and Angles (deg) for $[Pt_2Na(\mu\text{-dpnapy})_3(XylNC)_2](PF_6)$·$2CH_2Cl_2$·$2H_2O$ (4a·$2CH_2Cl_2$·$2H_2O$)

Pt(1)−P(1)	2.297(4)	Pt(2)−P(2)	2.313(4)
Pt(1)−P(3)	2.315(4)	Pt(2)−P(4)	2.292(3)
Pt(1)−P(5)	2.296(3)	Pt(2)−P(6)	2.288(4)
Pt(1)−C(1)	1.97(2)	Pt(2)−C(2)	1.94(1)
Na(1)−N(11)	2.44(1)	Na(1)−N(12)	2.44(1)
Na(1)−N(21)	2.46(1)	Na(1)−N(22)	2.45(1)
Na(1)−N(31)	2.45(1)	Na(1)−N(32)	2.46(1)
N(1)−C(1)	1.20(2)	N(2)−C(2)	1.19(2)
N(1)−C(11)	1.39(2)	N(2)−C(21)	1.41(2)
P(1)−Pt(1)−P(3)	109.8(1)	P(2)−Pt(2)−P(4)	112.2(1)
P(1)−Pt(1)−P(5)	110.8(1)	P(2)−Pt(2)−P(6)	110.7(1)
P(1)−Pt(1)−C(1)	113.9(4)	P(2)−Pt(2)−C(2)	102.3(4)
P(3)−Pt(1)−P(5)	111.9(1)	P(4)−Pt(2)−P(6)	109.5(1)
P(3)−Pt(1)−C(1)	102.5(4)	P(4)−Pt(2)−C(2)	107.9(4)
P(5)−Pt(1)−C(1)	107.8(4)	P(6)−Pt(2)−C(2)	114.1(4)
Pt(1)−C(1)−N(1)	172(1)	Pt(2)−C(2)−N(2)	173(1)
C(1)−N(1)−C(11)	174(1)	C(2)−N(2)−C(21)	170(2)
N(11)−Na(1)−N(12)	55.3(3)	N(21)−Na(1)−N(22)	55.9(4)
N(31)−Na(1)−N(32)	55.7(4)		

environments, and each is ligated by three P atoms of dpnapy ligands (average Pt(1)−P = 2.303 Å, average Pt(2)−P = 2.298 Å) and an isocyanide carbon atom (Pt1−C1 = 1.97(2) Å, Pt2−C2 = 1.94(1) Å). The average P−Pt−C and P−Pt−P angles are 108.1 and 110.8°, respectively, demonstrating that each platinum(0) center has tetrahedral geometry with 18 valence electrons. Although several metallocryptates capped by trigonal d^{10} metals with 16-valence-electron configurations have been reported as complexes **1** and **2**, complex **4a** is the first example of a PNNP metallocryptate capped by electron-rich d^{10} metals with 18 valence electrons. The Pt−P bond distances are appreciably longer by ca. 0.1 Å in comparison with those of $[Pt(CO)(PPh_3)_3]$ (average

Pt−P = 2.22 Å)[10] and [(dfepe)Pt(CO)]$_2$(μ-dfepe) (average Pt−P = 2.19 Å, dfepe = $(C_2F_5)_2PCH_2CH_2P(C_2F_5)_2$),[11] due presumably to the steric crowdedness of the phenyl groups of dpnapy as well as the rigidness of the double-tripodal $\{(dpnapy)_3Na\}^+$ unit. The Pt atoms reside significantly above the planes defined by their coordinated P atoms by 0.72 Å (Pt1) and 0.71 Å (Pt2), resulting in the long Pt···Na and Pt···Pt separations (Pt1···Na1 = 4.244(5) Å, Pt2···Na2 = 4.237(5) Å, Pt1···Pt2 = 8.4601(7) Å), compared with $[Au_2Na(\mu\text{-dpnapy})_3](PF_6)_3$ (**2a**) (average Au···Na = 3.564 Å, Au···Au = 7.126(2) Å).[7] The terminal XylNC ligands are linearly attached to the platinum atoms along the Pt−Na−Pt axis (Pt(1)−C(1)−N(1) = 172(1)°, Pt(2)−C(2)−N(2) = 173(1)°).

The complex cation of **4b** is isostructural with that of **4a**:[12] average Pd···Na = 4.228 Å, average Na−N = 2.47 Å, average Pd−P = 2.347 Å, average Pd−C = 2.02 Å, average N−C = 1.17 Å, average P−Pd−C = 107.9°, and average P−Pd−P = 110.9°. A slight difference was observed in the bond distances to the Pd centers; the Pd−P and Pd−C bond lengths are longer than the corresponding values in **4a**, implying that the Pd centers are less electron-rich and the back-bonding interaction with the terminal isocyanides might be weaker than that in the diplatinum(0) analogue **4a**.

Reactions of $[M_2Na(\mu\text{-dpnapy})_3(XylNC)_2](PF_6)$ (M = Pt (4a), Pd (4b)) with CO. The terminal isocyanide ligands of **4a**,**b** were readily replaced by CO (1 atm) to afford reddish violet crystals of $[M_2Na(\mu\text{-dpnapy})_3(CO)_2](PF_6)$ (M = Pt (**4c**), Pd (**4d**)), which were characterized by spectroscopic techniques (Scheme 1). The IR spectrum of **4d** exhibited a terminal CO stretching vibration at 1968 cm^{-1}, and the ^{1}H NMR spectrum of the aromatic region indicated a symmetrical environment of the three dpnapy ligands, where the naphthyridine protons appeared as two doublets at δ 7.64 and 6.91 ppm with $^3J_{HH}$ = 8.3 Hz. The ^{31}P{^{1}H} NMR spectrum of **4d** showed a singlet peak at δ 25.0 ppm. These spectral features suggest that the symmetrical dipalladium(0) metallocryptate with a sodium ion is capped by terminal CO ligands in **4d**. In contrast, the IR spectrum of the Pt analogue **4c** exhibited two intense C≡O stretching bands at 1961 and 1943 cm^{-1}, attributable to terminal carbonyl ligands coordinated to Pt(0) centers. The ^{31}P{^{1}H} spectrum of the reaction solution predominantly containing **4c** under a CO atmosphere showed two doublets at δ 22.2 and 23.5 ppm accompanied by ^{195}Pt satellite peaks with $^1J_{PtP}$ = 3683 and 3854 Hz, respectively.[12] The spectrum indicated the presence of two nonequivalent P atoms with a ratio of 1:1, which are surprisingly coupled with J_{PP} = 34 Hz, despite the fact that the two P atoms of dpnapy are separated by ca. 7.6 Å. These spectral patterns were not variable even at elevated temperature up to 50 °C. In light of these spectra, complex **4c** consists of the diplatinum(0) metallocryptate $[Pt_2Na(\mu\text{-dpnapy})_3(CO)_2]^+$ asymmetrically capped by two carbonyls with different extents of back-donating interactions with Pt(0) centers. Presumably, one carbonyl attached more strongly to a Pt center causes a slight structural change around the metal, which may influence the other Pt site through the rigid metallocryptate framework and result in stabilization of the asymmetric structure.

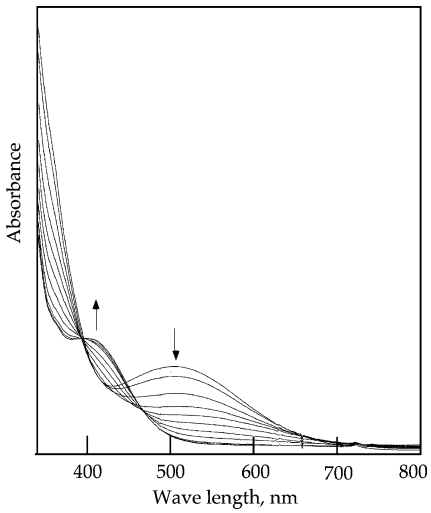

Figure 4. UV−vis spectral changes of **4a** by titration with 0.2 equiv portions of HPF_6 in dichloromethane.

Successive Encapsulation of Acidic Hydrides into the Cage of $[Pt_2Na(\mu\text{-dpnapy})_3(XylNC)_2]^+$ (4a) Leading to $[Pt_2Na(H)(\mu\text{-dpnapy})_3(XylNC)_2]^{2+}$ (5) and $[Pt_2Na(H)_2(\mu\text{-dpnapy})_3(XylNC)_2]^{3+}$ (6). When complex **4a** was treated with HPF_6 in dichloromethane (titrating by addition of 0.2 equiv portions), the absorption spectral patterns quickly varied as shown in Figure 4, in which two successive processes were clearly demonstrated with isosbestic points at 395 and 463 nm. These transformations were unambiguously characterized as $[Pt_2Na(\mu\text{-dpnapy})_3(XylNC)_2]^+$ (**4a**) → $[Pt_2Na(H)(\mu\text{-dpnapy})_3(XylNC)_2]^{2+}$ (**5**) → $[Pt_2Na(H)_2(\mu\text{-dpnapy})_3(XylNC)_2]^{3+}$ (**6**), by isolation of the respective compounds as described below (Scheme 1). Complexes $[Pt_2Na(H)(\mu\text{-dpnapy})_3(XylNC)_2](PF_6)_2$ (**5**) and $[Pt_2Na(H)_2(\mu\text{-dpnapy})_3(XylNC)_2](PF_6)_3$ (**6**) were alternatively synthesized by reactions of the zerovalent triplatinum(0) cluster $[Pt_3(XylNC)_6]$ with $NaPF_6$ and dpnapy in the presence of regulated amounts of HPF_6.

The IR spectrum of **6** showed one N≡C stretching vibration at 2148 cm^{-1}, the value being shifted to the higher energy side by ca. 100 cm^{-1} in comparison with that of **4a** and falling within the range for terminal isocyanides attached to Pt(I) centers.[13] The IR spectrum of complex **5** showed two kinds of N≡C stretching bands at 2143 and 2051 cm^{-1}; the former is comparable to that of **6** and the latter to that of **4a**. The ^{1}H NMR spectrum of **6** showed a hydride peak at δ −11.15 ppm with ^{195}Pt satellites ($^1J_{PtH}$ = 337 Hz), a singlet for *o*-methyl protons of xylyl units at δ 1.74 ppm, and two doublets for symmetrical naphthyridine protons at δ 6.97 and 8.23 ppm ($^3J_{HH}$ = 8.3 Hz), in a ratio of 1:6:3:3 (Figure 5b). The ^{31}P{^{1}H} NMR spectrum indicated a singlet resonance for the P atoms of dpnapy ligands at δ 20.4 ppm with $^1J_{PtP}$ = 2969 Hz (Figure 1c). The reduced Pt−P coupling constant suggests that the Pt centers are oxidized to some extent. In the ^{1}H NMR spectrum of **5**,

(10) (a) Albano, V. G.; Ricci, G. M. B.; Bellon, P. L. *Inorg. Chem.* **1969**, *8*, 2109. (b) Albano, V. G.; Bellon, P. L.; Sansoni, M. *J. Chem. Soc., Chem. Commun.* **1969**, 899.

(11) Peters, R. G.; Bennett, B. L.; Roddick, D. M. *Inorg. Chim. Acta* **1997**, *265*, 205.

(12) See Supporting Information.

(13) (a) Yamamoto, Y.; Yamazaki, H. *Organometallics* **1993**, *12*, 933. (b) Tanase, T.; Ukaji, H.; Kudo, Y.; Ohno, M.; Kobayashi, K.; Yamamoto, Y. *Organometallics* **1994**, *13*, 1374.

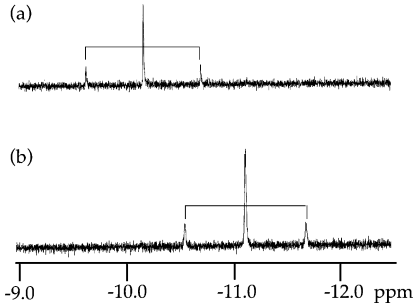

Figure 5. ^{1}H NMR spectra for the hydride regions of (a) **5** and (b) **6** in CD_2Cl_2 at room temperature.

a hydride peak was observed at δ −10.18 ppm ($^1J_{PtH}$ = 326 Hz) and two singlet peaks for *o*-methyl protons of isocyanide ligands were found at δ 1.73 and 1.91 ppm in a 1:1 ratio (Figure 5a). It should be noted that the value of the $^1J_{PtH}$ coupling constant is remarkably small for the terminal hydrides bound to Pt atoms and also for bridging hydrides.[13b,14] Although the aromatic region was rather complicated and suggested an asymmetric structure of the metallocryptate, the peak integration ratio indicated the presence of the Pt-bound hydride, XylNC, and dpnapy in a 1:2:3 ratio. The $^{31}P\{^1H\}$ NMR of complex **5** exhibited two resonances for nonequivalent P atoms at δ 24.6 ppm ($^1J_{PtP}$ = 3904 Hz) and 20.5 ppm ($^1J_{PtP}$ = 3017 Hz) (Figure 1b). On the basis of chemical shifts and coupling constants compared with those of **4a** and **6**, the former (δ 24.6 ppm) is assignable to the P atoms bound to the Pt(0) center and the latter (δ 20.5 ppm) to those coordinated to the PtH metal center (Figure 1). These spectral features clearly demonstrate that an acidic hydride is fixed on a platinum center of the $[Pt_2Na(dpnapy)_3(XylNC)_2]^+$ metallocryptate and were unchanged up to 50 °C. The ESI mass spectra of **5** and **6** in dichloromethane showed parent peaks at *m/z* 1085.73 and 724.19 corresponding to $[Pt_2Na(H)(dpnapy)_3(XylNC)_2]^{2+}$ and $[Pd_2Na(H)_2(dpnapy)_3(XylNC)_2]^{3+}$, respectively. The electronic absorption spectra of complexes **5** and **6** were entirely different from that of **4a** (Figure 2), which showed a weak broad band at 534 nm ($\epsilon = 4.04 \times 10^3$) (**5**) and a moderate broad band at 403 nm ($\epsilon = 1.17 \times 10^4$) (**6**), in addition to the characteristic absorptions of dpnapy around 280−340 nm. These spectral features were reflected in the UV−vis spectral changes given in Figure 4.

When the dihydride complex **6** was treated with an excess amount of Et_3N in CH_2Cl_2, the electronic absorption spectrum slowly changed, as shown in Figure 6, which was monitored by every 10 min. The absorption of **6** around 400 nm decreased initially and, instead, the characteristic band of **4a** appeared around 500 nm via the intervening band around 530 nm of **5**, these corresponding to the stepwise hydride elimination processes of **6** → **5** → **4a**. It should be apparent that the rate of the first step, **6** → **5**, is much faster than that for the second step, **5** → **4a**. These observations implied the existence of long-range influence on the hydride elimination between the two separated Pt sites.

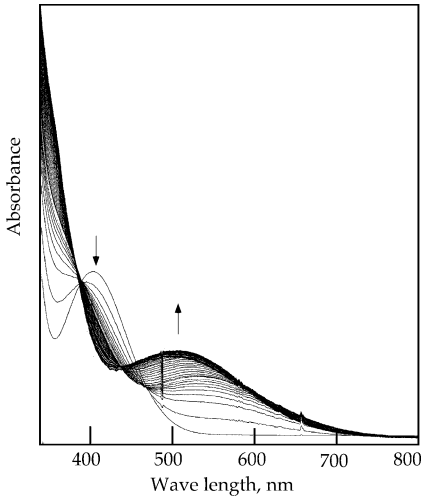

Figure 6. UV−vis spectral changes for the reaction of **6** with an excess amount of Et_3N (~300 equiv) in dichloromethane at room temperature monitored every 10 min.

The Pd analogue **4b** did not show the successive encapsulation of acidic hydrides such as **4a** and decomposed by treatment with HPF_6. It is notable that Pd−hydride complexes are relatively rare, owing to unstable Pd−H bonds in comparison with Pt−hydride complexes.[15]

Structures of $[Pt_2Na(H)(\mu\text{-dpnapy})_3(XylNC)_2]^{2+}$ (5) and $[Pt_2Na(H)_2(\mu\text{-dpnapy})_3(XylNC)_2]^{3+}$ (6). The structures of $[Pt_2Na(H)(\mu\text{-dpnapy})_3(XylNC)_2](PF_6)_2$ (**5**) and $[Pt_2Na(H)_2(\mu\text{-dpnapy})_3(XylNC)_2](PF_6)_3$ (**6**) were determined by X-ray crystallographic analyses. Perspective views for the complex cations of **5** and **6** are illustrated in Figures 7 and 8, and selected bond distances and angles are listed in Tables 2 and 3, respectively. Structural parameters around the metal centers are summarized in Table 4.

The asymmetric unit of **6** contains one complex cation of $[Pt_2Na(H)_2(\mu\text{-dpnapy})_3(XylNC)_2]^{3+}$ and three hexafluorophosphate anions without any direct interactions between them. The complex cation has a structure essentially similar to that of **4a** and is comprised of the pseudo-D_3 helical metallocryptate $\{Pt_2Na(\mu\text{-dpnapy})_3(XylNC)_2\}^+$, in which two protons are incorporated as acidic hydrides bound to the Pt centers (Figure 8). The positions of the hydrogen atoms were determined by difference Fourier syntheses (it should be noted that the hydrogen atom positions are not supported definitively by X-ray diffraction analysis). To each Pt center, the hydrogen atom attached from the opposite side of the capping isocyanide with an average Pt−H bond length of 1.59 Å and average C−Pt−H angle of 174.5°; the hydrogen is incorporated in the small cavity constituted by the $\{Pt(PCN)_3Na\}$ framework and is fixed onto the electron-rich tetrahedral Pt(0) center. The present hydride binding onto the monomeric Pt(0) center is notably unprecedented. The Pt−H bonds are slightly tilted with respect to the Pt−Na−Pt axis with Pt1−H91−Na = 175(4)° and Pt2−H92−Na1 = 166(4)°. The Na···H distances are 2.34(6) Å (Na1−H91) and 2.35(6) Å (Na1−

(14) For example: (a) Tulip, T. H.; Yamagata, T.; Yoshida, T.; Wilson, R. D.; Ibers, J. A.; Otsuka, S. *Inorg. Chem.* **1979**, *18*, 2239. (b) Bracher, G.; Grove, D. M.; Venanzi, L. M.; Bachechi, F.; Mura, P.; Zambonelli, L. *Angew. Chem., Int. Ed. Engl.* **1978**, *17*, 778. (c) Carmona, D.; Thouvenot, R.; Vananzi, L. M.; Bachechi, F.; Zambonelli, L. *J. Organomet. Chem.* **1983**, *250*, 589. (d) Reinartz, S.; Baik, M.-H.; White, P. S.; Brookhart, M.; Templeton, J. L. *Inorg. Chem.* **2001**, *40*, 4726.

(15) Cotton, F. A.; Wilkinson, G. *Advanced Inorganic Chemistry*, 4th ed.; Wiley-VCH: New York, 1987; Chapter 27.

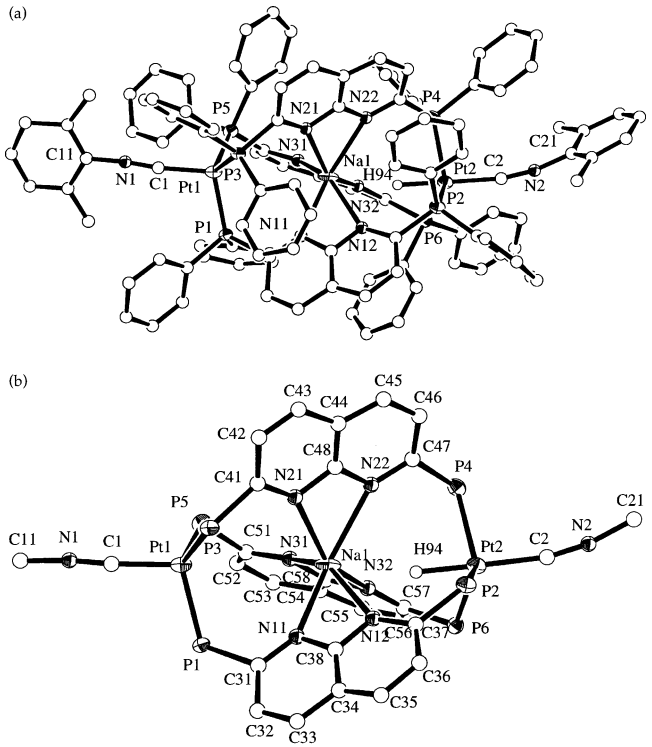

Figure 7. (a) ORTEP plot for the complex cation of **5**·2CH_2Cl_2·0.5H_2O, $[Pt_2Na(H)(\mu\text{-dpnapy})_3(XylNC)_2]^{2+}$. The carbon and nitrogen atoms are drawn with ideal circles for clarity. (b) ORTEP view for the complex framework of **5**, the phenyl and xylyl rings being omitted for clarity.

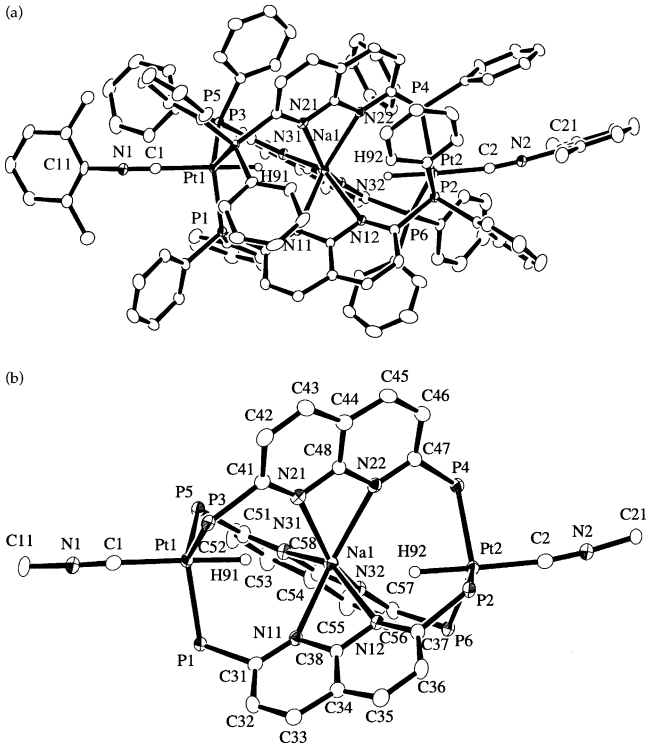

Figure 8. (a) ORTEP plot for the complex cation of **6**·1.5CH_2Cl_2·Et_2O·0.5H_2O, $[Pt_2Na(H)_2(\mu\text{-dpnapy})_3(XylNC)_2]^{3+}$. (b) ORTEP view for the complex framework of **6**, the phenyl and xylyl rings being omitted for clarity.

H92), suggesting no direct bonding interaction between them. Whereas the small Pt−H coupling constant ($^1J_{PtH}$ = 337 Hz) in the ^1H NMR spectrum of **6** was suggestive of a weak Pt−H bonding interaction, the present novel encapsulating structure might increase the stability of the Pt-bound acidic hydrides by preventing access of reactive species from outside. In comparison with the structure of **4a**, appreciable deformation was observed around the platinum atoms. After the hydride was captured, the Pt atom deformed slightly toward trigonal-bipyramidal geometry with an average P−Pt−P angle of 117.0° (110.8° for **4a**) and average C−Pt−P angle of 100.2° (108.1° for **4a**). The Pt atoms sit above the P_3 triangular planes by 0.41 Å and are dragged by 0.3 Å toward the inside of the cage upon the hydride encapsulation. The Pt···Na and Pt···Pt distances are reduced to 3.928(2) Å (Pt1···Na1), 3.907(2) Å (Pt2···Na1), and 7.8331(3) Å (Pt1···Pt2) according to the inward drag. The average Pt−P and Pt−C bond lengths of 2.341 and 2.005 Å are longer than those of **4a**, which may lead to definite elongation of the Na−N bond distances (2.476(4)-2.524(4) Å, average 2.498 Å).

Compound **5** was composed of the complex cation of $[Pt_2Na(H)(\mu\text{-dpnapy})_3(XylNC)_2]^{2+}$ and two hexafluorophosphate counteranions. The structure of the complex cation has the same metallocryptate framework as

Table 2. Selected Bond Lengths (Å) and Angles (deg) for $[Pt_2Na(H)(\mu\text{-dpnapy})_3(XylNC)_2](PF_6)_2$·2$CH_2Cl_2$·0.5$H_2O$ (5·2CH_2Cl_2·0.5H_2O)

Pt(1)−P(1)	2.310(4)	Pt(2)−P(2)	2.328(4)
Pt(1)−P(3)	2.308(4)	Pt(2)−P(4)	2.327(4)
Pt(1)−P(5)	2.316(4)	Pt(2)−P(6)	2.344(4)
Pt(1)−C(1)	1.92(2)	Pt(2)−C(2)	1.95(2)
Na(1)−N(11)	2.40(1)	Na(1)−N(12)	2.52(1)
Na(1)−N(21)	2.43(1)	Na(1)−N(22)	2.54(1)
Na(1)−N(31)	2.42(1)	Na(1)−N(32)	2.57(1)
N(1)−C(1)	1.19(2)	N(2)−C(2)	1.20(2)
N(1)−C(11)	1.39(3)	N(2)−C(21)	1.42(2)
Pt(1)−H(94)	1.66		
P(1)−Pt(1)−P(3)	113.0(1)	P(2)−Pt(2)−P(4)	116.5(1)
P(1)−Pt(1)−P(5)	112.4(1)	P(2)−Pt(2)−P(6)	116.6(2)
P(1)−Pt(1)−C(1)	104.8(5)	P(2)−Pt(2)−C(2)	98.4(5)
P(3)−Pt(1)−P(5)	113.0(2)	P(4)−Pt(2)−P(6)	115.4(1)
P(3)−Pt(1)−C(1)	112.3(5)	P(4)−Pt(2)−C(2)	97.0(5)
P(5)−Pt(1)−C(1)	100.4(5)	P(6)−Pt(2)−C(2)	108.9(5)
Pt(1)−C(1)−N(1)	169(2)	Pt(2)−C(2)−N(2)	168(1)
C(1)−N(1)−C(11)	174(1)	C(2)−N(2)−C(21)	169(1)
N(11)−Na(1)−N(12)	53.6(4)	N(21)−Na(1)−N(22)	55.1(4)
N(31)−Na(1)−N(32)	54.4(4)		

Table 3. Selected Bond Lengths (Å) and Angles (deg) for $[Pt_2Na(H)_2(\mu\text{-dpnapy})_3(XylNC)_2](PF_6)_3$·1.5$CH_2Cl_2$·$Et_2O$·0.5$H_2O$ (6·1.5CH_2Cl_2·Et_2O·0.5H_2O)

Pt(1)−P(1)	2.330(1)	Pt(2)−P(2)	2.351(1)
Pt(1)−P(3)	2.351(1)	Pt(2)−P(4)	2.336(1)
Pt(1)−P(5)	2.335(1)	Pt(2)−P(6)	2.341(1)
Pt(1)−C(1)	2.004(5)	Pt(2)−C(2)	2.006(5)
Na(1)−N(11)	2.480(4)	Na(1)−N(12)	2.524(4)
Na(1)−N(21)	2.517(4)	Na(1)−N(22)	2.499(4)
Na(1)−N(31)	2.476(4)	Na(1)−N(32)	2.490(4)
N(1)−C(1)	1.149(6)	N(2)−C(2)	1.157(7)
N(1)−C(11)	1.408(6)	N(2)−C(21)	1.413(7)
Pt(1)−H(91)	1.59(6)	Pt(2)−H(92)	1.59(6)
P(1)−Pt(1)−P(3)	115.57(5)	P(2)−Pt(2)−P(4)	113.22(5)
P(1)−Pt(1)−P(5)	121.94(5)	P(2)−Pt(2)−P(6)	116.12(5)
P(1)−Pt(1)−C(1)	96.9(1)	P(2)−Pt(2)−C(2)	99.5(1)
P(3)−Pt(1)−P(5)	113.38(5)	P(4)−Pt(2)−P(6)	121.59(4)
P(3)−Pt(1)−C(1)	107.8(1)	P(4)−Pt(2)−C(2)	94.4(1)
P(5)−Pt(1)−C(1)	96.1(1)	P(6)−Pt(2)−C(2)	106.2(1)
Pt(1)−C(1)−N(1)	170.1(5)	Pt(2)−C(2)−N(2)	172.3(4)
C(1)−N(1)−C(11)	173.0(5)	C(2)−N(2)−C(21)	174.2(5)
N(11)−Na(1)−N(12)	54.6(1)	N(21)−Na(1)−N(22)	54.7(1)
N(31)−Na(1)−N(32)	55.1(1)		

Table 4. Structural Parameters for the Metal Atoms of 4a·2CH_2Cl_2·2H_2O, 5·2CH_2Cl_2·0.5H_2O, and 6·1.5CH_2Cl_2·Et_2O·0.5H_2O

	4a		5		6	
	Pt1	Pt2	Pt1	Pt2	Pt1	Pt2
Pt−P_{av}, Å	2.303	2.298	2.311	2.333	2.339	2.343
Pt−C, Å	1.97	1.94	1.92	1.95	2.004	2.006
P−Pt−P_{av}, deg	110.8	110.8	112.8	116.2	117.0	117.0
P−Pt−C_{av}, deg	108.1	108.1	105.8	101.4	100.3	100.0
Pt−P_3 plane, Å[a]	0.72	0.71	0.63	0.46	0.41	0.41
Pt···Na, Å	4.224(5)	4.237(5)	4.013(8)	4.086(8)	3.928(2)	3.907(2)
Pt···Pt, Å	8.4601(7)		8.099(1)		7.8331(3)	
Na−N_{av}, Å	2.45	2.45	2.42	2.54	2.491	2.504

[a] Deviation of the Pt atoms from the plane defined by the three P atoms.

found in **4a** and **6**, in which a hydrogen atom attaches to one Pt center to form an asymmetric structure (Figure 7). The Pt1 atom is ligated by three phosphorus atoms of dpnapy and an isocyanide carbon atom in a distorted-tetrahedral geometry, compared with the structure of **4a**. The average P−Pt1−C and P−Pt1−P angles are 105.8 and 112.8°, respectively, and the average Pt1−P bond length is 2.311 Å. In contrast, the Pt2 atom is surrounded by the three P atoms of dpnapy, the C atom of XylNC, and the hydrogen atom H94 with average P−Pt2−C and P−Pt2−P angles of 101.4 and 116.2°, respectively. The average Pt2−P distance is 2.333 Å, and the Pt2−H94 bond length is 1.66 Å. The structure around the Pt2 atom is appreciably deformed toward a trigonal-bipyramidal geometry, in comparison with that of the Pt1 atom, and is essentially similar to that in **6**. The Pt1 and Pt2 atoms deviate outward from the P_3 triangular planes by 0.63 and 0.46 Å, respectively, and the Pt···Na and Pt···Pt interatomic distances fall between the values of **4a** and **6** (Pt1···Na1 = 4.013(8) Å, Pt2···Na1 = 4.086(8) Å, and Pt1···Pt2 = 8.099(1) Å). The asymmetric structure of **5** reveals the nondynamic fixation of the hydride, which is consistent with the spectroscopic features, and further brings about the definite distortion around the central Na atom with average Na1−N distance of 2.42 Å for the Pt1 side (Pt(0)) and 2.54 Å for the Pt2 side (PtH). The structural distortion around the Pt2 site influenced the partner Pt1 site to be slightly deformed and less reactive, consequently resulting in stabilization of the asymmetric structure of **5**. In other words, the distortion caused by the hydride encapsulation on one Pt site could come down to the other Pt center through the rigid metallocryptate framework, which can be recognized as "*steric communication*" in a small molecule.

Redox Properties of Complexes 4a, 5, and 6. In general, oxidation states of metals involved in M−H units can be varied depending on the hydrogen being anionic, neutral, or cationic, as well as auxiliary ligands surrounding the metal centers. To examine the oxidation states of the Pt centers, X-ray photoelectron spectroscopic analyses were carried out on complexes **4a**, **5**, and **6**. The binding energy for Pt $4f_{7/2}$ and $4f_{5/2}$ states of **4a**, **5**, and **6** and the reference platinum complexes are given in Table 5. The binding energies for complex **4a,** containing two Pt(0) centers, showed equivalent platinum atoms with 71.6 eV ($4f_{7/2}$) and 75.0 eV ($4f_{5/2}$), and those for complex **6** with two PtH units were 73.4 eV ($4f_{7/2}$) and 76.7 eV ($4f_{5/2}$). The values of complex **6** are very close to those of the platinum(I) dimer [Pt^I_2(dppm)$_2$-(XylNC)$_2$](PF_6)$_2$[13a] (73.1 eV ($4f_{7/2}$), 76.4 eV ($4f_{5/2}$)), rather than the platinum(II) monomer [Pt^{II}(dppe)(XylNC)$_2$]-(PF_6)$_2$[16] (74.2 eV ($4f_{7/2}$), 77.5 eV ($4f_{5/2}$)) (dppm = bis-(diphenylphosphino)methane, dppe = 1,2-bis(diphenylphosphino)ethane), suggesting that the Pt(I) oxidation state of the Pt−H units was actually established in **6** through one-electron migration from the Pt(0) center to the hydrogen. This is in agreement with the stretching vibration energy of the N≡C groups observed in the IR spectrum of **6**. The XPS spectrum of the asymmetric complex **5** exhibited two sets of binding energies at 71.6 ($4f_{7/2}$), 74.9 eV ($4f_{5/2}$) and 73.3 ($4f_{7/2}$), 76.7 eV ($4f_{5/2}$) in an integration ratio of ca. 1:1, the former being comparable to the Pt(0) state demonstrated with complex **4a** and the latter to the Pt(I) state as observed in complex **6**.

Table 5. Binding Energies (eV) for Complexes 4a, 5, and 6, [Pt_2(μ-dppm)$_2$(XylNC)$_2$](PF_6)$_2$, and [Pt(dppe)(XylNC)$_2$](PF_6)$_2$[a]

complex	$4f_{7/2}$	$4f_{5/2}$
4a	71.6	75.0
5	71.6, 73.3[b]	74.9, 76.7[b]
6	73.4	76.7
[Pt_2(μ-dppm)$_2$(XylNC)$_2$](PF_6)$_2$	73.1	76.4
[Pt(dppe)(XylNC)$_2$](PF_6)$_2$	74.2	77.5

[a] Legend: dppm = bis(diphenylphosphino)methane, dppe = 1,2-bis(diphenylphosphino)ethane. [b] Observed in 41:59 integration ratio.

The cyclic voltammograms (CVs) of complexes **4a**, **5**, and **6** in dichloromethane are shown in Figure 9. The CV of **4a** showed two irreversible oxidation waves at $E_{pa}{}^1 = -0.14$ V and $E_{pa}{}^2 = 0.15$ V (vs Ag/$AgPF_6$), and the coulometric analyses indicated that each process involved one-electron oxidation of the platinum center. These results suggest that the $Pt^0{}_2$ complex **4a** undergoes two irreversible one-electron oxidation processes abbreviated as $Pt^0Pt^0 \rightarrow Pt^IPt^0 \rightarrow Pt^IPt^I$, while some concomitant structural changes may be involved in each process and are not elucidated at present. The relatively large separation of the peak potentials ($\Delta E_{pa} = 0.29$ V) indicates the presence of a stable Pt^IPt^0 intermediate species, due presumably to a long-range electronic communication between the two Pt centers. Most of the electronic communication systems reported have been ascribed to electron delocalization effects for mixed-valence states,[17] and in contrast, the present system may include the steric mechanism, as evidenced in the hydride encapsulation process, although electronic factors were not ruled out. The CV of complex **5**, including Pt(0) and Pt(I)H centers, exhibited only a one-electron

(16) Appleton, T. G.; Bennett, M. A.; Tomkins, I. B. *J. Chem. Soc., Dalton Trans.* **1976**, 439.

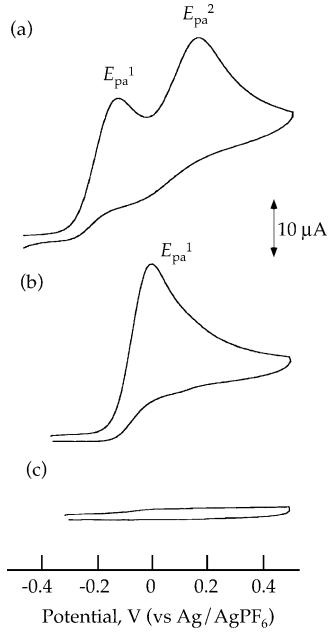

Figure 9. Cyclic voltammograms of **4a**, **5**, and **6** in dichloromethane containing 0.1 M [nBu$_4$N][PF$_6$] with a scan rate of 100 mV/s.

oxidation wave at $E_{pa}^1 = -0.01$ V, presumably corresponding to $Pt^0(Pt^IH) \rightarrow Pt^I(Pt^IH)$, and that of complex **6** with two Pt(I)H units showed no redox process in the potential window (Figure 9). These observations revealed that the encapsulation of an acidic hydride in the metallocryptate [Pt$_2$Na(μ-dpnapy)$_3$(XylNC)$_2$]$^+$ made the hydride-bound Pt center redox inactive in a stepwise fashion.

Conclusion

In this study, electron-rich diplatinum(0) and dipalladium(0) complexes, [M$_2$Na(μ-dpanpy)$_3$L$_2$](PF$_6$) (M = Pt, L = XylNC (**4a**), CO (**4c**); M = Pd, L = XylNC (**4b**), CO (**4d**)), were successfully synthesized and characterized, where the double-tripodal unit of {(dpnapy)$_3$Na}$^+$ was capped by the M^{0}L fragments to establish an 18-valence-electron configuration. In particular with [Pt$_2$Na(μ-dpanpy)$_3$(XylNC)$_2$](PF$_6$) (**4a**), novel successive encapsulation of acidic hydrides into the cage was readily promoted, leading to the mono- and dihydride complexes [Pt$_2$Na(H)(μ-dpanpy)$_3$(XylNC)$_2$](PF$_6$)$_2$ (**5**) and [Pt$_2$Na(H)$_2$(μ-dpanpy)$_3$(XylNC)$_2$](PF$_6$)$_3$ (**6**). The detailed structural examination revealed the steric communication mechanism between the long-separated Pt centers, which should be responsible for the stability of the asymmetric complex of **5**. A similar mechanism was presumed to be evident in the two irreversible, one-electron oxidation processes of **4a**, and interestingly, the hydride encapsulation caused the Pt center to be redox silent, suggesting that the electrochemical behavior of **4a** can be switched by the stepwise hydride masking.

Experimental Section

General Procedures. All manipulations were carried out under a nitrogen atmosphere with standard Schlenk techniques. Reagent grade solvents were dried by standard procedures and were freshly distilled prior to use. 2,7-Bis(diphenylphosphino)-1,8-naphthyridine (dpnapy)[5] and [Pt$_3$(XylNC)$_6$][18] were prepared by the known methods, and [Pt(XylNC)$_4$](PF$_6$)$_2$ was prepared according to a modified procedure of ref 19. NaPF$_6$ was recrystallized from ethyl acetate. IR spectra were recorded on a Jasco FT/IR-410 spectrophotometer, and electronic absorption spectra were acquired on Shimadzu UV-3100 and Hewlett-Packard Agilent 8453 spectrophotometers. ^{1}H and ^{31}P{^{1}H} NMR spectra were recorded on a Varian Gemini 2000 spectrometer at 300 and 121 MHz, respectively. ^{1}H NMR spectra were referenced to residual protio solvent or to TMS as external standard, and ^{31}P{^{1}H} NMR spectra were referenced to 85% H$_3$PO$_4$ as external standard. X-ray photoelectron spectroscopy (XPS) was carried out on a Shimadzu Axis-Ultra with monochromated Al Kα radiation (1486.6 eV). Electrochemical measurements were performed with a Hokuto-Denko HZ-3000 system using 1 mM dichloromethane solutions of the samples (**4a**, **5**, and **6**) containing 0.1 M [nBu$_4$N][PF$_6$] as supporting electrolyte and using a standard three-electrode cell consisting of a Ag/AgPF$_6$ reference electrode, platinum wire as the counter electrode, and glassy carbon as the working electrode. Controlled-potential electrolysis was performed with the same instrument using a platinum-mesh working electrode. ESI-TOF mass spectra were recorded on an Applied Biosystems Mariner high-resolution mass spectrometer with positive ionization mode.

Preparation of [Pt$_2$Na(μ-dpnapy)$_3$(XylNC)$_2$](PF$_6$)·0.5CH$_2$Cl$_2$ (4a·0.5CH$_2$Cl$_2$). The complex [Pt(XylNC)$_4$](PF$_6$)$_2$ (51 mg, 0.051 mmol) and dpnapy (41 mg, 0.082 mmol) were dissolved in CH$_2$Cl$_2$ (10 mL), and the mixture was stirred for 30 min at room temperature. The solvent was evaporated to dryness, and the residue was reduced with NaBH$_4$ (5.4 mg, 0.14 mmol) in EtOH (5 mL) with stirring for 2 h. The solvent was removed by the cannula technique, and the violet residue was extracted with CH$_2$Cl$_2$ (15 mL). The solution was concentrated to 2 mL, and diethyl ether (ca. 2 mL) was carefully added. When the mixture was cooled to 2 °C, violet microcrystals of [Pt$_2$Na(μ-dpnapy)$_3$(XylNC)$_2$](PF$_6$)·0.5CH$_2$Cl$_2$ (**4a**·0.5CH$_2$Cl$_2$) were obtained, which were separated by filtration, washed with diethyl ether, and dried under vacuum (31 mg, yield 52% with respect to Pt). Anal. Calcd for C$_{114.5}$H$_{91}$N$_8$P$_7$F$_6$ClPt$_2$Na: C, 58.31; H, 3.89; N, 4.75. Found: C, 58.35; H, 3.84; N, 4.88. IR (KBr, cm^{-1}): 2048 (N≡C), 841 (PF$_6$). UV−vis (in CH$_2$Cl$_2$, nm (ϵ, M^{-1} cm^{-1})): 507 (1.13×10^4), 318 (6.71×10^4). ^{1}H NMR (300 MHz, room temperature, CD$_2$Cl$_2$): δ 1.95 (s, 12H, o-Me), 6.3−7.4 (m, 78H, Ar), 6.43 (d, 6H, $^3J_{HH}$ = 8.3 Hz), 7.40 (d, 6H, $^3J_{HH}$ = 8.3 Hz). ^{31}P{^{1}H} NMR (121 MHz, room temperature, CD$_2$Cl$_2$): δ 23.3 (s, 6P, $^1J_{PtP}$ = 3850 Hz). ESI-MS (in CH$_2$Cl$_2$): m/z 1020.19 (z2, {[Pt$_2$Na(dpnapy)$_3$(XylNC)] + H}$^{2+}$ (1020.21)). Recrystallization from a dichloromethane/diethyl ether mixed solvent afforded thin platelike crystals of **4a**·2CH$_2$Cl$_2$·2H$_2$O which were suitable for X-ray crystallography.

Preparation of [Pd$_2$Na(μ-dpnapy)$_3$(XylNC)$_2$](PF$_6$)·3.5CH$_3$OH (4b·3.5CH$_3$OH). Portions of dpnapy (104 mg, 0.209 mmol) and NaPF$_6$ (17 mg, 0.10 mmol) were dissolved in a CH$_2$Cl$_2$/CH$_3$OH (7:3) mixed solvent (10 mL) and stirred for 2 h. The solvent was evaporated to dryness, and the residue was dissolved in 20 mL of dichloromethane, to which [Pd$_3$(XylNC)$_6$] (53 mg, 0.048 mmol) was added. The color of the solution immediately turned to dark violet from pale yellow. The solution was concentrated, and diethyl ether (ca. 1.5 mL) was carefully added. When the mixture was cooled to 2 °C, violet crystals of [Pd$_2$Na(μ-dpnapy)$_3$(XylNC)$_2$](PF$_6$)·3.5CH$_3$OH (**4b**·

(17) (a) Narvor, N. L.; Toupet, L.; Lapinte, C. *J. Am. Chem. Soc.* **1995**, *117*, 7129. (b) Brady, M.; Weng, W.; Zhou, Y.; Seyler, J. W.; Amoroso, A. J.; Arif, A. M.; Bohme, M.; Frenking, G.; Gladysz, J. A. *J. Am. Chem. Soc.* **1997**, *119*, 775. (c) Kheradmandan, S.; Heinze, K.; Schmalle, H. W.; Berke, H. *Angew. Chem., Int. Ed.* **1999**, *38*, 2270. (d) Ren, T.; Zou, G.; Alvarez, J. C. *Chem. Commun.* **2000**, 1197. (e) Tanase, T.; Matsuo, J.; Onaka, T.; Begum, R. A.; Hamaguchi, M.; Yano, S.; Yamamoto, Y. *J. Organomet. Chem*. **1999**, 592, 103; references therein.

(18) Green, M.; Howard, J. A.; Spencer, J. L.; Stone, F. G. A. *J. Chem. Soc., Chem. Commun.* **1975**, 3.

(19) Miller, J. S.; Balch, A. L. *Inorg. Chem.* **1972**, *11*, 2069.

3.5CH_3OH) were obtained. The crystals were separated by filtration, washed with diethyl ether, and dried under vacuum (76 mg, yield 48% with respect to Pd). Anal. Calcd for $C_{117.5}H_{104}O_{3.5}N_8P_7F_6Pd_2Na$: C, 62.70; H, 4.66; N, 4.98. Found: C, 62.45; H, 4.63; N, 5.15. IR (KBr, cm^{-1}): 2061 (N≡C), 840 (PF_6). UV−vis (in CH_2Cl_2, nm (ϵ, M^{-1} cm^{-1})): 505 (8.20×10^3), 314 (5.97×10^4). ^1H NMR (300 MHz, room temperature, CD_2Cl_2): δ 1.94 (s, 12H, *o*-Me), 6.3−7.7 (m, 78H, Ar), 6.54 (d, 6H, $^3J_{HH}$ = 8.4 Hz), 7.47 (d, 6H, $^3J_{HH}$ = 8.4 Hz). $^{31}P\{^1H\}$ NMR (121 MHz, room temperature, DMF-d_7): δ 26.7 (s, 6P). ESI-MS (in CH_2Cl_2): *m/z* 1731.25 (*z*1, $[Pd_2Na(dpnapy)_3]^+$ (1731.22)). Recrystallization from a dichloromethane/diethyl ether mixed solvent afforded thin platelike crystals of **4b**·3CH_2Cl_2·4H_2O which were suitable for X-ray crystallography.

Preparation of [$Pt_2Na(\mu$-dpnapy$)_3(CO)_2$][PF_6]·CH_2Cl_2 (4c·CH_2Cl_2). [$Pt_2Na(\mu$-dpnapy$)_3$(XylNC$)_2$](PF_6)·0.5CH_2Cl_2 (**4a**·0.5CH_2Cl_2, 15.6 mg, 6.61×10^{-3} mmol) was dissolved in CH_2Cl_2 (4 mL), and CO (1 atm) was introduced into the flask. After bubbling of CO for 12 min, the solution was concentrated to 2 mL. Addition of diethyl ether (ca. 0.5 mL) afforded red crystals of [$Pt_2Na(\mu$-dpnapy$)_3(CO)_2$](PF_6)·CH_2Cl_2 (**4c**·CH_2Cl_2), which were separated by filtration, washed with diethyl ether, and dried under vacuum (yield 18%, 2.6 mg). Anal. Calcd for $C_{99}H_{74}O_2N_6P_7F_6Cl_2Pt_2Na$: C, 54.18; H, 3.40; N, 3.83. Found: C, 54.06; H, 3.36; N, 4.15. IR (KBr, cm^{-1}): 1961, 1943 (C≡O), 839 (PF_6). UV−vis (in CH_2Cl_2, nm (ϵ, M^{-1} cm^{-1})): 457 (8.78×10^3), 310 (4.94×10^4), 278 (5.20×10^4 (sh)). $^{31}P\{^1H\}$ NMR (121 MHz, room temperature, CD_2Cl_2): δ 22.2 (d, 3P, $^1J_{PtP}$ = 3683 Hz, $J_{PP'}$ = 34 Hz), 23.5 (d, 3P, $^1J_{PtP}$ = 3854 Hz, $J_{PP'}$ = 34 Hz).

Preparation of [$Pd_2Na(\mu$-dpnapy$)_3(CO)_2$][PF_6]·1.5CH_2Cl_2·Et_2O (4d·1.5CH_2Cl_2·Et_2O). [$Pd_2Na(\mu$-dpnapy$)_3$(XylNC$)_2$](PF_6)·3.5CH_3OH (**4a**·3.5CH_3OH, 32 mg, 0.014 mmol) was dissolved in CH_2Cl_2 (7 mL), and CO (1 atm) was introduced into the flask. After bubbling of CO for 20 min, the solution was concentrated. Addition of Et_2O (ca. 1 mL) afforded red crystals of [$Pd_2Na(\mu$-dpnapy$)_3(CO)_2$](PF_6)·1.5CH_2Cl_2·Et_2O (**4d**·1.5CH_2Cl_2·Et_2O), which were separated by filtration, washed with diethyl ether, and dried under vacuum (yield 54%, 17 mg). Anal. Calcd for $C_{103.5}H_{85}O_3N_6P_7F_6Cl_3Pd_2Na$: C, 58.26; H, 4.02; N, 3.94. Found: C, 58.11; H, 4.23; N, 4.26. IR (KBr, cm^{-1}): 1983 sh, 1968 (C≡O), 839 (PF_6). UV−vis (in CH_2Cl_2, nm (ϵ, M^{-1} cm^{-1})): 495 (2.71×10^3), 313 (2.52×10^4), 267 (2.73×10^4 (sh)). ^1H NMR (300 MHz, room temperature, CD_2Cl_2): δ 6.4−8.5 (m, 78H, Ar), 6.91 (d, 6H, $^3J_{HH}$ = 8.3 Hz), 7.64 (d, 6H, $^3J_{HH}$ = 8.3 Hz). $^{31}P\{^1H\}$ NMR (121 MHz, room temperature, CD_2Cl_2): δ 25.0 (s, 6P).

Preparation of [$Pt_2Na(H)(\mu$-dpnapy$)_3$(XylNC$)_2$][PF_6]$_2$·0.5Et_2O (5·0.5Et_2O). Portions of $NaPF_6$ (37 mg, 0.22 mmol), HPF_6 (ca. 10×10^{-3} mmol), and dpnapy (73 mg, 0.15 mmol) were dissolved in 12 mL of a MeOH/CH_2Cl_2 (1:1) mixed solvent. A dichloromethane solution (6 mL) of [Pt_3(XylNC$)_6$] (48 mg, 0.035 mmol) was slowly added to the solution, and the mixture was stirred for 4 h at room temperature. After removal of the solvent under reduced pressure, the residue was extracted with CH_2Cl_2 (20 mL), and the extract was filtered to remove inorganic salts. The solution was concentrated to 3 mL, and diethyl ether (ca. 2 mL) was added to the solution. When the mixture was cooled to 2 °C, brown crystals of [$Pt_2Na(H)(\mu$-dpnapy$)_3$(XylNC$)_2$](PF_6)$_2$·0.5Et_2O (**5**·0.5Et_2O) were obtained. The crystals were separated by filtration, washed with diethyl ether, and dried under vacuum (yield 21% vs Pt, 27 mg). Anal. Calcd for $C_{116}H_{96}O_{0.5}N_8P_8F_{12}Pt_2Na$: C, 55.75; H, 3.87; N, 4.48. Found: C, 55.50; H, 4.26; N, 4.52. IR (KBr, cm^{-1}): 2143, 2051 (N≡C), 841 (PF_6). UV−vis (in CH_2Cl_2, nm (ϵ, M^{-1} cm^{-1})): 534 (4.04×10^3), 292 (4.89×10^4). ^1H NMR (300 MHz, room temperature, CD_2Cl_2): δ −10.2 (s, 1H, Pt−H, $^1J_{PtH}$ = 326 Hz), 1.73 (s, 6H, *o*-Me), 1.91 (s, 6H, *o*-Me), 6.3−7.9 (m, 78H, Ar). $^{31}P\{^1H\}$ NMR (121 MHz, room temperature, CD_2Cl_2): δ 20.5 (s, 3P, $^1J_{PtP}$ = 3017 Hz), 24.6 (s, 3P, $^1J_{PtP}$ = 3904 Hz). ESI-MS (in CH_2Cl_2): *m/z* 1085.73 (*z*2, $[Pt_2Na(H)(dpnapy)_3(XylNC)_2]^{2+}$ (1085.75)). Recrystallization from a dichloromethane/diethyl ether mixed solvent afforded needlelike crystals of **5**·2CH_2Cl_2·0.5H_2O which were suitable for X-ray crystallography.

Table 6. Crystallographic and Experimental Data for [$M_2Na(\mu$-dpnapy$)_3$(XylNC$)_2$](PF_6)·solv (M = Pt (4a·2CH_2Cl_2·2H_2O), Pd (4b·3CH_2Cl_2·4H_2O))

	4a·2CH_2Cl_2·2H_2O	**4b**·3CH_2Cl_2·4H_2O
formula	$C_{116}H_{98}N_8P_7F_6Cl_4O_2Pt_2Na$	$C_{117}H_{104}N_8P_7F_6Cl_6O_4Pd_2Na$
fw	2521.89	2465.47
cryst syst	triclinic	triclinic
space group	$P\bar{1}$ (No. 2)	$P\bar{1}$ (No. 2)
a, Å	15.2297(9)	15.366(1)
b, Å	19.8498(7)	19.9417(4)
c, Å	21.980(2)	22.096(2)
α, deg	71.112(6)	70.81(1)
β, deg	88.849(3)	88.80(2)
γ, deg	70.010(1)	70.33(1)
V, Å^3	5904.5(7)	5990(1)
Z	2	2
T, °C	−120	−120
D_{calcd}, g cm^{-3}	1.418	1.367
abs coeff, cm^{-1}	26.06	5.93
2θ range, deg	$6 < 2\theta < 52$	$6 < 2\theta < 49$
no. of unique data	20662	21621
no. of obsd data	11526 ($I > 2.5\sigma(I)$)	6209 ($I > 3\sigma(I)$)
no. of variables	1316	728
data/param	8.76	8.53
R^a	0.080	0.104
$R_w{}^a$	0.089	0.115

^{a} $R = \sum||F_o| - |F_c||/\sum|F_o|$; $R_w = [\sum w(|F_o| - |F_c|)^2/\sum w|F_o|^2]^{1/2}$ ($w = 1/\sigma^2(F_o)$).

Preparation of [$Pt_2Na(H)_2(\mu$-dpnapy$)_3$(XylNC$)_2$][PF_6]$_3$·0.5CH_2Cl_2 (6·0.5CH_2Cl_2). [Pt_3(XylNC$)_6$] (19 mg, 0.014 mmol) was added to a solution containing $NaPF_6$ (15 mg, 0.092 mmol), HPF_6 (0.013 mmol), and dpnapy (46 mg, 0.092 mmol) in 15 mL of a MeOH/CH_2Cl_2 (1:2) mixed solvent. The reaction mixture was stirred for 12 h, and then the solvent was removed under reduced pressure. The residue was extracted with CH_2Cl_2 (15 mL). After filtration, the extract was concentrated to 0.5 mL and MeOH (5 mL) was added to the solution. Diethyl ether (0.5 mL) was layered on the solution, which was allowed to stand at 2 °C to afford yellow needlelike crystals of [$Pt_2Na(H)_2(\mu$-dpnapy$)_3$(XylNC$)_2$](PF_6)$_3$·0.5CH_2Cl_2 (**6**·0.5CH_2Cl_2). The crystals were separated by filtration, washed with diethyl ether, and dried under vacuum (yield 33% vs Pt, 18 mg). Anal. Calcd for $C_{114.5}H_{93}N_8P_9ClF_{18}Pt_2Na$: C, 51.89; H, 3.54; N, 4.23. Found: C, 51.95; H, 3.76; N, 4.26. IR (KBr, cm^{-1}): 2148 (N≡C), 839 (PF_6). UV−vis (in CH_2Cl_2, nm (ϵ, M^{-1} cm^{-1})): 403 (1.17×10^4), 283 (5.56×10^4). ^1H NMR (300 MHz, room temperature, CD_2Cl_2): δ −11.15 (s, 2H, Pt−H, $^1J_{PtH}$ = 337 Hz), 1.74 (s, 12H, *o*-Me), 6.5−8.2 (m, 78H, Ar), 6.97 (d, 6H, $^3J_{HH}$ = 8.3 Hz), 8.23 (d, 6H, $^3J_{HH}$ = 8.3 Hz). $^{31}P\{^1H\}$ NMR (121 MHz, room temperature, CD_2Cl_2): δ 20.4 (s, 6P, $^1J_{PtP}$ = 2969 Hz). ESI-MS (in CH_2Cl_2): *m/z* 724.19 (*z*3, $[Pt_2Na(H)_2(dpnapy)_3(XylNC)_2]^{3+}$ (724.17)). Recrystallization from a dichloromethane/diethyl ether mixed solvent afforded block-shaped crystals of **6**·1.5CH_2Cl_2·Et_2O·0.5H_2O which were suitable for X-ray crystallography.

X-ray Crystallographic Analyses of 4a·2CH_2Cl_2·2H_2O, 4b·3CH_2Cl_2·4H_2O, 5·2CH_2Cl_2·0.5H_2O, and 6·1.5CH_2Cl_2·Et_2O·0.5H_2O. Crystal data and experimental conditions are summarized in Tables 6 and 7. All data were collected at −120 °C on a Rigaku AFC8R/Mercury CCD diffractometer equipped with graphite-monochromated Mo Kα radiation using a rotating-anode X-ray generator. A total of 1440 oscillation images, covering the whole sphere of $2\theta < 52°$, were collected with exposure rates of 120 (**4a**, **6**), 240 (**4b**), and 480° s^{-1} (**5**) by the ω-scan method ($-70 < \omega < 110°$) with a $\Delta\omega$ value of 0.25°. The crystal-to-detector (70 × 70 mm) distance was set to 60 mm. The data were processed using the Crystal Clear 1.3.5 program (Rigaku/MSC)[20] and corrected for Lorentz−polariza-

Table 7. Crystallographic and Experimental Data for $[Pt_2Na(H)(\mu\text{-dpnapy})_3(XylNC)_2](PF_6)_2\cdot 2CH_2Cl_2\cdot 0.5H_2O$ ($5\cdot 2CH_2Cl_2\cdot 0.5H_2O$) and $[Pt_2Na(H)_2(\mu\text{-dpnapy})_3(XylNC)_2](PF_6)_3\cdot 1.5CH_2Cl_2\cdot Et_2O\cdot 0.5H_2O$ ($6\cdot 1.5CH_2Cl_2\cdot Et_2O\cdot 0.5H_2O$)

	$5\cdot 2CH_2Cl_2\cdot 0.5H_2O$	$6\cdot 1.5CH_2Cl_2\cdot Et_2O\cdot 0.5H_2O$
formula	$C_{116}H_{96}N_8P_8F_{12}Cl_4O_{0.5}Pt_2Na$	$C_{119.5}H_{106}N_8P_9F_{18}Cl_3O_{1.5}Pt_2Na$
fw	2640.84	2818.47
cryst syst	triclinic	monoclinic
space group	$P\bar{1}$ (No. 2)	$P2_1/n$ (No. 14)
a, Å	17.0841(9)	23.0221(7)
b, Å	18.063(2)	28.1459(8)
c, Å	18.5949(8)	18.2233(5)
α, deg	83.871(8)	
β, deg	74.999(8)	90.151(1)
γ, deg	89.986(9)	
V, Å^3	5508.8(6)	11808.3(6)
Z	2	4
T, °C	−120	−120
D_{calcd}, g cm^{-3}	1.592	1.585
abs coeff, cm^{-1}	28.17	26.33
2θ range, deg	$6 < 2\theta < 52$	$6 < 2\theta < 52$
no. of unique data	19847	23558
no. of obsd data	7793 ($I > 3\sigma(I)$)	16992 ($I > 2\sigma(I)$)
no. of variables	749	1087
data/param	10.40	11.61
R^a	0.069	0.037
R_w or wR2	0.081[b]	0.116[c]

[a] $R = \sum||F_o| - |F_c||/\sum|F_o|$. [b] $R_w = [\sum w(|F_o| - |F_c|)^2/\sum w|F_o|^2]^{1/2}$ ($w = 1/\sigma^2(F_o)$). [c] $wR2 = [\sum w(F_o^2 - F_c^2)^2/\sum w(F_o)^2]^{1/2}$ (for all data, $w = 1/[\sigma^2(F_o) + (0.0601P)^2 + 0.0205P]$, $P = (F_o^2 + 2F_c^2)/3$).

tion and absorption effects. The structure of $\mathbf{4a}\cdot 2CH_2Cl_2\cdot 2H_2O$ was solved by direct methods (SIR92)[21] and refined on F with full-matrix least-squares techniques with teXsan.[22] All non-hydrogen atoms were refined with anisotropic thermal parameters, and the positions of hydrogen atoms were calculated and fixed in the refinement. The structure of $\mathbf{4b}\cdot 3CH_2Cl_2\cdot 4H_2O$ was solved by heavy-atom methods (DIRDIF94 Patty).[23] The Pd, Cl, P, Na, and F atoms were refined anisotropically, and other non-hydrogen atoms were refined with isotropic temperature factors. All hydrogen atoms except those of solvent molecules were calculated and fixed in the refinement. The structure of $\mathbf{5}\cdot 2CH_2Cl_2\cdot 0.5H_2O$ was solved by direct methods (SIR92). The Pt, P, Na, and F atoms were refined anisotropically, and other non-hydrogen atoms were refined with isotropic thermal parameters; the solvated molecules were refined with disordered models. The C−H hydrogen atoms, except those of solvent molecules, were calculated, and the position of the Pt-bound H94 was determined by difference Fourier synthesis. The structure of $\mathbf{6}\cdot 1.5CH_2Cl_2\cdot Et_2O\cdot 0.5H_2O$ was solved by direct methods (SIR92) and refined on F^2 by least-squares techniques with SHELXL-97.[24] The non-hydrogen atoms were refined with anisotropic thermal parameters, and the C−H hydrogen atoms were placed at calculated positions and were fixed in the refinement. The positions of the hydride H atoms (H91, H92) were determined from difference Fourier maps and refined isotropically. All calculations were carried out on a Silicon Graphics O2 station with the teXsan crystallographic software package and a Pentium PC with the Crystal Structure package.[25]

Acknowledgment. This work was partly supported by Grant-in-Aid for Scientific Research from Ministry of Education, Culture, Sports, Science, and Technology of Japan.

Supporting Information Available: Tabulation of X-ray crystallographic data for **4a**,**b**, **5**, and **6**, including text giving experimental details, tables giving atomic parameters and bond distances and angles, and an ORTEP plot of complex **4b**, ESI mass spectra for the parent peaks of complexes **4a**, **5**, and **6** with their simulated spectra, the $^{31}P\{^1H\}$ NMR spectrum of complex **4c**, and the X-ray photoelectron spectrum for complex **5** with curve-fitted spectra. This material is available free of charge via the Internet at http://pubs.acs.org.

OM049548V

(20) Crystal Clear 1.3.5: Operating software for the CCD detector system; Rigaku and Molecular Structure Corp., 2003.
(21) Altomare, A.; Burla, M. C.; Camalli, M.; Cascarano, M.; Giacovazzo, C.; Guagliardi, A.; Polidori, G. *J. Appl. Crystallogr.* **1994**, *27*, 435.
(22) TEXSAN: Crystal Structure Analysis Package; Molecular Structure Corp., 1999.
(23) Beurskens, P. T.; Admiraal, G.; Beurskens, G.; Bosman, W. P.; de Gelder, R.; Israel, R.; Smits, J. M. M. DIRDIF-94 Program System; Technical Report of the Crystallography Laboratory; University of Nijmegen, Nijmegen, The Netherlands, 1994.
(24) Sheldrick, G. M. SHELXL-97: Program for the Refinement of Crystal Structures; University of Göttingen, Göttingen, Germany, 1996.
(25) Crystal Structure 3.6: Crystal Structure Analysis Package; Rigaku and Molecular Structure Corp., 2003.